NANO LETTERS

pubs.acs.org/NanoLett

Letter

Utilizing Gate-Controlled Supercurrent for All-Metallic Tunable Superconducting Microwave Resonators

Younghun Ryu, Jinhoon Jeong, Junho Suh, Jihwan Kim, Hyoungsoon Choi,* and Jinwoong Cha*

Cite This: https://doi.org/10.1021/acs.nanolett.3c04080

Read Online

ACCESS | Metrics & More | Article Recommendations

ABSTRACT: Hybridizing a microwave mode with a quantum state requires precise frequency matching of a superconducting microwave resonator and the corresponding quantum object. However, fabrication always brings imperfections in geometry and material properties, causing deviations from the desired operating frequencies. An effective and universal strategy for their resonant coupling is to tune the frequency of a resonator, as quantum states like phonons are hardly tunable. Here, we demonstrate gate-tunable, titanium-nitride (TiN)-based superconducting resonators by implementing a nanowire inductor whose kinetic inductance is tuned via the gate-controlled supercurrent (GCS) effect. We investigate their responses for different gate biases and observe 4% (∼150 MHz) frequency tuning with decreasing internal quality factors. We also perform temperature-controlled experiments to support phonon-related mechanisms in the GCS effect and the resonance tuning. The GCS effect-based method proposed in this study provides an effective route for locally tunable resonators that can be employed in various hybrid quantum devices.

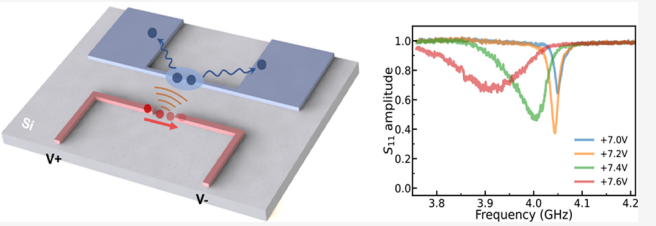

KEYWORDS: *gate-controlled supercurrent, kinetic inductance, tunable microwave resonator, superconducting nanowire*

Microwave resonators are indispensable components in superconducting quantum devices.[1−3] Equipping resonators with frequency tunability enhances the versatility of superconducting devices, enabling, for example, tunable microwave parametric amplifiers[4−6] and tunable couplers.[7] Also, resonant coupling of microwave modes with other quantum states like spins,[8−10] phonons,[11−13] and magnons[14−16] in various hybrid quantum systems requires the ability to precisely tune the frequency of superconducting resonators. Existing methods for frequency tuning mainly utilize the flux tunability of Josephson junctions (JJ) or the kinetic inductance (KI) of superconducting nanowires. JJ-based devices have demonstrated a wide range of frequency tuning. However, their dynamic range is limited by the relatively low critical current of JJs and realizing a high-quality JJ requires sophisticated fabrication techniques such as angle evaporation and in situ oxidation.[17,18] In contrast, the KI-based devices rely on the inherent nonlinear inductance of superconducting nanowires to tune their frequencies by flowing a direct current (DC). However, since this approach requires a relatively high current (∼mA) flowing through a large area of circuits, it is challenging to implement a local control without affecting the nearby superconducting circuit elements.

Recent studies have demonstrated tunable superconducting resonators with locally tunable elements. For example, JJs based on hybrid semiconductor−superconductor nanostructures have been used to realize voltage-tunable superconducting qubits[19−21] and near-quantum limited parametric amplifiers.[22,23] This type of JJ allows for tuning the junction resistance with a gate voltage, thereby changing a JJ's critical current and, in turn, its Josephson inductance ($L_J = \hbar/(2eI_c)$). Another promising approach utilizes a junction made of a semiconducting nanowire in contact with superconducting electrodes.[24−26] This component takes advantage of voltage-tunability of the electron density and the induced superconducting gap of the nanowire, enabling gate-tunable resonance[27] and gate-tunable parametric amplifier.[28] Despite their potential, such hybrid platforms require the growth of high-quality materials and complex fabrication processes.

The gate-controlled supercurrent (GCS) effect,[29−42] which induces the suppression of the superconductivity of materials under a gate bias, might provide alternative solutions to achieve tunable microwave resonators. This effect has been reported in devices made of titanium nanowire[29] as well as other various superconductors.[31,35,39,40,42] The microscopic origin of the GCS effect remains elusive, and several possible mechanisms behind the GCS effect have been proposed. These include the direct electric field effect,[29−31,35−39] the injection of

Received: October 23, 2023
Revised: January 10, 2024
Accepted: January 10, 2024

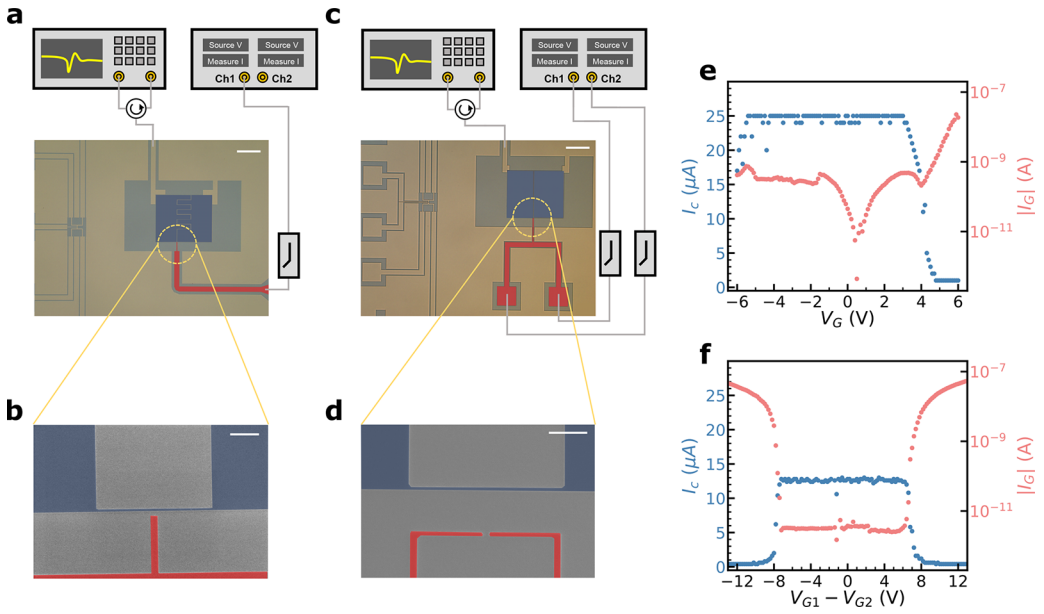

Figure 1. Optical microscope images of (a) type 1 and (b) type 2 devices. Scale bar, 500 μm. S_{11} spectra are measured using a vector network analyzer with a cryogenic circulator. DC gate lines are filtered with a series of RC and RF filters. Scanning electron microscope images of the nanowire junctions in (b) type 1 and (d) type 2 devices. Scale bar, 1 μm. The critical current, I_c, and the gate leakage current, $|I_G|$, as a function of the gate voltages, (e) V_G for type 1 and (f) $V_{G1} - V_{G2}$ for type 2, respectively.

hot electrons,[40,41,43] phonon-induced heating,[34,42] and the injection of out-of-equilibrium phonons.[33] The GCS effect in microwave regime has recently been demonstrated by coplanar-waveguide superconducting microwave resonators implementing nanojunctions,[34,41] but the range of frequency tuning is limited to a few megahertz. Here, we fabricate lumped-element microwave resonators implementing titanium nitride (TiN) nanowires and demonstrate enhanced frequency tuning up to ∼150 MHz, which corresponds to 4% of their resonance frequencies, via the GCS effect. We also explore the dominant mechanism for the GCS effect in our devices.

To explore the GCS effect, we fabricate two different superconducting microwave resonators, type 1 and type 2, made of TiN as shown in Figure 1a,c. The fabrication of our devices begins with a reactive sputtering of a 20 nm thick TiN layer on a high-resistivity silicon wafer ($\rho > 10^4$ Ω·cm). Note that highly resistive silicon is well-known for its low microwave loss, and TiN nanowires on highly resistive silicon substrates have recently been employed to demonstrate the GCS effect.[33,40] To define the geometry of the resonators, we perform 50 keV e-beam lithography followed by an inductively coupled plasma reactive ion etching process with SF_6 chemistry.[44] Both devices comprise a planar capacitor with a 4 μm gap and an 80 nm wide, 4 μm long nanowire junction as a superconducting inductor (Figure 1b and Figure 1d). The capacitance values are estimated to be 0.6 pF for type 1 and 0.3 pF for type 2 from Sonnet simulations. The nanowire's kinetic inductance is in the 2−3 nH range. We position the nanowire close to a gate electrode (marked in red in Figure 1b and Figure 1d) to control its kinetic inductance via the GCS effect. The geometry of our circuits enhances the contribution of the nanowire inductance to the microwave resonance for efficient gate tuning. The type 1 device is designed to have a typical side-gate structure where the separation of a nanowire and a gate electrode is 150 nm (Figure 1a). In the type 2 device, a nanowire is positioned 1.1 μm away from two remote gate electrodes to reduce the field effect in the nanowire. Also, the gap between the two electrodes is designed to have a 160 nm gap so that hot electrons mainly travel through the gap with a minimized gate leakage to the nanowire. Such an arrangement for the type 2 device allows us to explore the most dominant mechanism behind the GCS effect for our devices, which is likely related to high-energy phonons originating from the relaxation of the hot electrons flowing through the electrode gap.[33]

To study the DC responses of the TiN nanowires, we fabricate an additional nanowire device for 4-probe measurements on each sample and characterize its critical current, I_c, and the gate leakage current, I_G, for different gate voltages. Note that the dimensions of the nanowire are identical with those in a microwave resonator on the same chip. Through this configuration, we successfully observe the signatures of the GCS effect such as the suppression of supercurrent flow as in previous studies.[29,30,36−39,42] In the type 1 device, we simply apply a voltage, V_G, to the single gate electrode. In the type 2 device with two gate electrodes, we apply V_{G1} to the first electrode and V_{G2} to the second electrode. From the DC measurements, we obtain $I_c = 25$ μA for type 1 (Figure 1e) and $I_c = 12.8$ μA for type 2 (Figure 1f) when no gate voltage is applied. We also extract the nanowire resistances of both devices (4754 Ω for type 1 and 6213 Ω for type 2, respectively) above the critical currents. Both type 1 and type 2 exhibit similar trends in response to the gate voltage. The suppression of I_c occurs with the onset of the gate leakage above certain values of the gate voltages, and a bipolar behavior with respect to the gate voltages is also present. These findings agree well with the results reported in previous studies.[29,30,36−39,42]

We characterize the microwave responses of our devices by measuring S_{11} parameters using a vector network analyzer at a 10 mK temperature (Figure 1a,c). We perform circle fits[45] considering in-phase and quadrature components of S_{11} to study how the resonance frequency, $f_r = (2\pi\sqrt{(L_g + L_k)C})^{-1}$,

https://doi.org/10.1021/acs.nanolett.3c04080
Nano Lett. XXXX, XXX, XXX−XXX

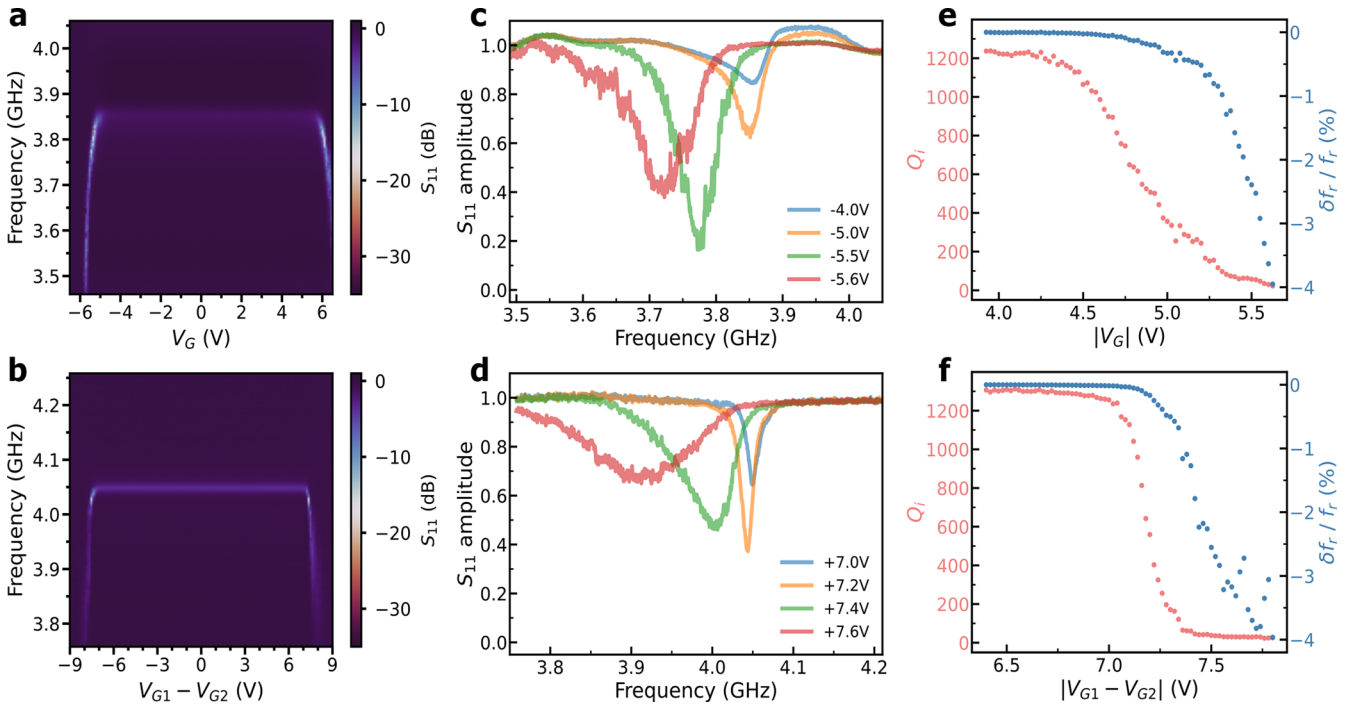

Figure 2. Colormaps showing the normalized S_{11} spectra as a function of the gate voltages, (a) V_G for type 1 and (b) $V_{G1} - V_{G2}$ for type 2, respectively. S_{11} spectra at four different gate voltages for (c) type 1 and (d) type 2. The resonance frequency change, $\delta f_r/f_r$, and the internal quality factor, Q_i, as a function of the gate voltages, (e) $|V_G|$ for type 1 and (f) $|V_{G1} - V_{G2}|$ for type 2.

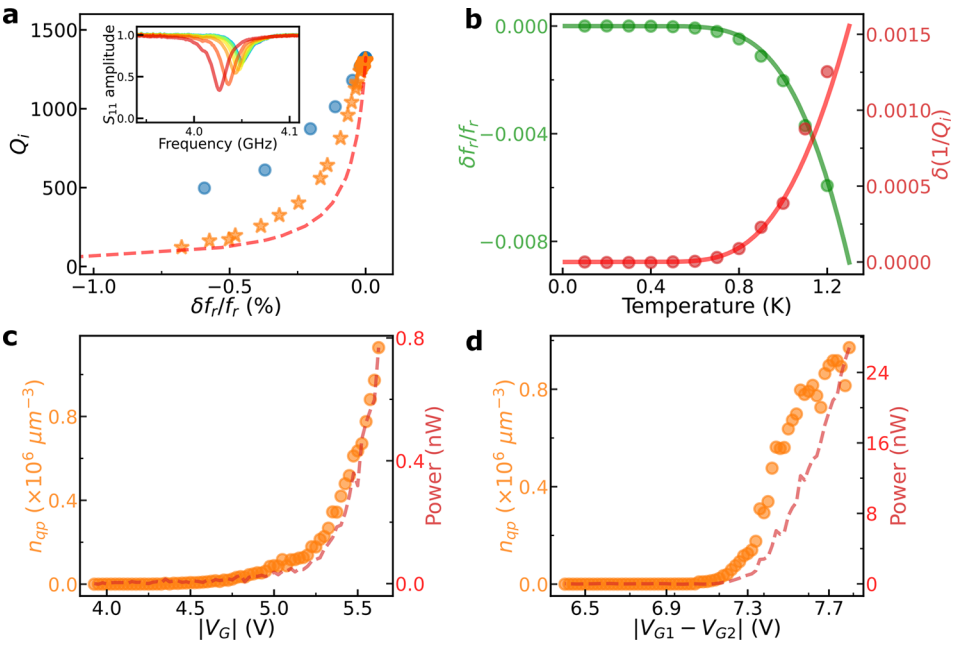

Figure 3. (a) Resonance frequency change, $\delta f_r/f_r$, versus the internal quality factor, Q_i, from gate-controlled (orange stars) and temperature-controlled microwave measurements (blue dots) and a theoretical estimation based on the Mattis−Bardeen equation considering pair-breaking effects at $T = 10$ mK for type 2. (b) $\delta f_r/f_r$ (green dots) and $\delta(1/Q_i)$ (red dots) as a function of temperature for type 2. The green and red solid lines show the fitting curves with the Mattis−Bardeen equation. $T_c = 3.63$ K is obtained from the fitting. Evaluated quasiparticle density, n_{qp}, and the power dissipation, P, as a function of the gate voltages, (c) $|V_G|$ for type 1 and (d) $|V_{G1} - V_{G2}|$ for type 2.

and the internal quality factor, Q_i, vary with V_G. Note that L_g and C represent the geometric inductance and the geometric capacitance of a resonator, respectively. L_k denotes the kinetic inductance of a nanowire and is expressed as

$$\frac{\hbar R_n}{\pi \Delta} \tanh^{-1}\left(\frac{\Delta}{2k_B T}\right)$$

in thermal equilibrium according to the Mattis−Bardeen theory,[46] where $\hbar$ is the reduced Planck constant, R_n is the normal resistance of a nanowire, Δ is a superconducting gap

https://doi.org/10.1021/acs.nanolett.3c04080
Nano Lett. XXXX, XXX, XXX−XXX

energy, k_B is the Boltzmann constant, and T is a temperature. The GCS effect due to the gating affects L_k, thereby enabling tunable microwave resonance.

Figure 2a,b illustrates the normalized S_{11} spectra for type 1 and type 2 for different gate voltages. The microwave spectra also exhibit a bipolar distribution with respect to the gate voltages, as observed in the DC measurements. In addition, the change in the microwave responses of both devices coincides with the development of the gate leakage current. In the leakage region ($|V_G| > 5$ V for type 1 and $|V_{G1} - V_{G2}| > 7$ V for type 2), the resonance frequencies show a significant decrease. The type 1 (type 2) devices show a shift from $f_r = 3.87$ GHz ($f_r = 4.05$ GHz) to $f_r = 3.72$ GHz ($f_r = 3.89$ GHz). In Figure 2c (Figure 2d), we present the microwave responses from the type 1 (type 2) device at $V_G = -4.0$ V, -5.0 V, -5.5 V, and -5.6 V ($V_{G1} - V_{G2} = 7.0$ V, 7.2 V, 7.4 V, and 7.6 V). We observe decreases in resonance frequency as well as increases in line width for both devices as $|V_G|$ and $|V_{G1} - V_{G2}|$ increase. The variation of the resonance spectra might originate from quasiparticles generated from high-energy phonons in the nanowires, which reduces the superconducting gap with increasing L_k. In silicon substrate, the maximum phonon energy that can exist is ~66 meV,[47] and this implies that the energy relaxation of hot electrons in gate leakage with a few eV energies can generate a large number of high energy phonons. As a result, both the resonance frequency and the internal quality factor diminish.[48] We also perform quantitative analyses of the change in the resonance frequency and internal quality factor of the resonators (Figure 2e,f). Notably, we observe significant shifts in their resonance frequencies ($\delta f_r/f_r \sim 4\%$) within the voltage ranges of interest. This tuning range is comparable to the tuning range of previously reported kinetic inductance-based resonators.[49,50] However, the tuning comes at a cost: the internal quality factor presents a 98% reduction from its initial value. When Q_i decreases by half from the value at zero gate voltage, the frequency shifts are 4.9 MHz ($\delta f_r/f_r \sim 0.13\%$) for type 1 and 5.6 MHz ($\delta f_r/f_r \sim 0.14\%$) for type 2.

It is known that a temperature increase reduces the resonance frequency and the quality factor of a superconducting microwave resonator. To examine the response of our devices under the temperature effect and the GCS effect, we perform temperature-controlled microwave measurements on our type 2 device and compare the results to the responses from the gate-tuning experiments. We vary the temperature from 100 mK to 1.2 K with 100 mK steps. Figure 3a illustrates $\delta f_r/f_r$ versus Q_i obtained from temperature-controlled and gate-tuning experiments for the type 2 device. Notably, Q_i from gate-tuned microwave responses degrades rapidly compared with the temperature-controlled microwave responses. For instance, when Q_i decreases by half from the maximum, $\delta f_r/f_r$ is about 0.37% (0.14%) for the temperature-controlled (the gate-tuning) case. This discrepancy indicates that the tuning via the GCS effect might originate from high-energy nonequilibrium phonons rather than the heating effect.

To extract superconducting properties from $\delta f_r/f_r$ and Q_i, we employ a generalized Mattis−Bardeen equation[51,52] for the complex conductivity, $\sigma = \sigma_1 - i\sigma_2$, of a superconductor which includes pair-breaking effects. When $k_BT \ll \Delta$ and $\hbar\omega \ll \Delta$, σ_1 and σ_2 are given by

$$\frac{\sigma_1(n_{qp}, T)}{\sigma_n} = \frac{2\Delta_0}{\hbar\omega}\frac{n_{qp}}{N_0\sqrt{2\pi k_B T\Delta_0}}\sinh(\xi)K_0(\xi) \quad (1)$$

$$\frac{\sigma_2(n_{qp}, T)}{\sigma_n} = \frac{\pi\Delta_0}{\hbar\omega}\left[1 - \frac{n_{qp}}{2N_0\Delta_0}\left(1 + \sqrt{\frac{2\Delta_0}{\pi k_B T}}\,e^{-\xi}I_0(\xi)\right)\right] \quad (2)$$

Here, ξ is $\hbar\omega/(2k_BT)$, n_{qp} is the density of quasiparticles, Δ_0 is the superconducting gap energy at $T = 0$ K, ω is the angular frequency of interest, k_B is the Boltzmann constant, I_0 and K_0 are the zeroth order modified Bessel functions of first and second kinds, respectively, σ_n is the normal state conductivity and N_0 is the density of states of electrons at the Fermi level. For our TiN film, we use $N_0 = 4 \times 10^{10}$ eV$^{-1}\mu$m^{-3}.[53] In addition, as the bulk mean free path for TiN ($l_{mean,e} \sim 45$ nm)[54] is larger than the thickness of our TiN film ($d = 20$ nm), we can use a thin-film approximation ($l_{mean,e} \sim d$). Also, $l_{mean,e}$ is much smaller than the London penetration depth ($\lambda_L \sim 730$ nm)[55] and the superconducting coherence length ($\xi_0 = \frac{\hbar v_f}{\pi\Delta} \sim 400$ nm, v_f is Fermi velocity of order of 10^6 m/s). Thus, our TiN film is in the local (dirty) limit of a superconductor.[48,56] In this limit, the complex conductivity, σ, is related to δf_r and Q_i as[57]

$$\frac{\delta f_r}{f_r} = \frac{\alpha}{2}\frac{\delta\sigma_2}{\sigma_2} \qquad \frac{1}{Q_i} = \frac{1}{Q_{i,0}} + \alpha\frac{\delta\sigma_1}{\sigma_2} \quad (3)$$

Here, $Q_{i,0}$ represents the unperturbed internal quality factor, $\alpha = L_k/(L_k + L_g)$ is the kinetic inductance fraction estimated using Sonnet microwave simulations ($\alpha = 0.74$ and 0.82 for type 1 and type 2, respectively), and $\delta\sigma_n$ is the conductivity change due to external perturbations. To check the validity of the Mattis-Bardeen equation for our device, we fit $\delta f_r/f_r$ and Q_i versus the temperature with eqs 1 and 2 with the thermal quasiparticle density at temperature T, $n_{qp} = 2N_0\sqrt{2\pi k_B T\Delta_0}\,e^{-\Delta_0/k_BT}$ (Figure 3b). Superconducting critical temperature, T_c, is determined to be 3.63 K from the fitting with $\Delta_0 = 1.764k_BT_c$.

Based on eqs 1−3 and the extracted Δ_0, we estimate n_{qp} for different gate voltages (Figure 3c,d). Note that n_{qp} deviates from the quasi-particle density in thermal equilibrium. We also analyze the power dissipation due to the gate leakage, $P = I_GV_G$. The behavior of n_{qp} with the gate voltages shows a trend almost identical to that of P, suggesting the frequency shift due to the GCS effect arises from energy relaxation processes (Figure 3c and 3d). In addition, P in the type 2 device is approximately 10−30 times higher than P in the type 1 device in the tuning range (Figure 3d), because the emitted phonons need to travel over a longer distance in the type 2 device. These phonons are expected to present ballistic behaviors due to the mean free path (MFP) longer than the gate-nanowire distance in our devices (MFP is ~1 μm for silicon membranes[58] and $\gg$1 μm for bulk silicon[59]). Assuming that the nonequilibrium phonons propagate through the substrate in an isotropic manner, the incident phonon flux to the nanowire in the type 1 device is greater than the flux to the nanowire in type 2 device, leading to the larger power dissipation for the same amount of n_{qp}. This might explain qualitatively why higher power dissipation is required for the same amount of tuning in the type 2 device compared to type 1 device. Based on the estimated n_{qp}, we again calculate $\delta f_r/f_r$

https://doi.org/10.1021/acs.nanolett.3c04080
Nano Lett. XXXX, XXX, XXX−XXX

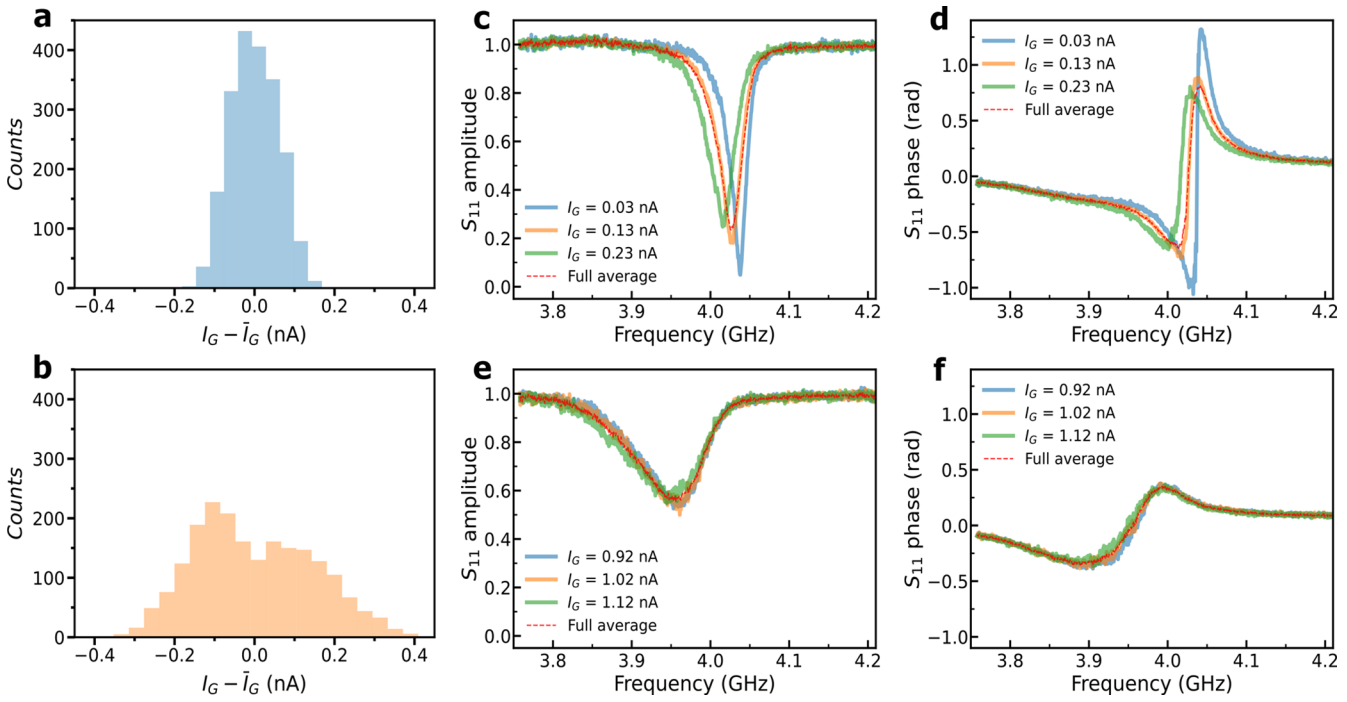

Figure 4. Current fluctuations measured at $V_{G1} - V_{G2}$ = (a) 7.3 and (b) 7.4 V, respectively. S_{11} spectra for three different gate leakage currents, I_G, at (c) $V_{G1} - V_{G2}$ = 7.3 and (e) 7.4 V, respectively. S_{11} phase spectra for three different gate leakage currents, I_G, at (d) $V_{G1} - V_{G2}$ = 7.3 and (f) 7.4 V, respectively. The spectra are obtained by averaging microwave responses within a 0.1 nA-sized current window for different values of I_G as the window center.

and Q_i of the type 2 device using the Mattias−Bardeen equation assuming T = 10 mK. These properties (red dashed curve in Figure 3a) from the theoretical calculation exhibit a slight deviation from the data from the GCS tuning experiment (orange stars in Figure 3a). This implies that the nanowire also experiences local heating in addition to pair-breaking processes due to nonequilibrium phonons.

We observe that the resonance spectra present fluctuations at high gate voltages (Figure 2c,d). Existing literature explains these fluctuations with nonequilibrium quasiparticles originating from high energy electron injection.[41] To study the origin of such fluctuations, we first examine the leakage current in the type 2 device at fixed gate voltages for 10 min. The measured leakage current is not constant, but exhibits fluctuations with levels of $\sigma_I \sim$ 25 pA at $V_{G1} - V_{G2}$ = 0 V, where σ_I is the standard deviation of a leakage current. σ_I remains constant until the onset of the leakage current at $V_{G1} - V_{G2}$ = 7.24 V ($\sigma_I \sim$ 26 pA). Above this point, the amount of current fluctuations increases to $\sigma_I \sim$ 58 pA at $V_{G1} - V_{G2}$ = 7.3 V (Figure 4a) and $\sigma_I \sim$ 147 pA at $V_{G1} - V_{G2}$ = 7.4 V (Figure 4b). The maximum current fluctuation ($\sigma_I \sim$ 264 pA) is observed at $V_{G1} - V_{G2}$ = 7.7 V, which is about 10 times larger than the current fluctuation at $V_{G1} - V_{G2}$ = 0 V. The current fluctuations remain unchanged before the onset of the leakage current. This supports that the current fluctuations are closely related to the GCS effect and do not originate from the resolution of our DC instruments. To investigate the impact of the leakage current fluctuations on the microwave responses, we analyze reflection spectra for three selected values of the leakage current, I_G = 0.03 nA, 0.13 nA and 0.23 nA (I_G = 0.92 nA, 1.02 nA and 1.12 nA), which are measured at $V_{G1} - V_{G2}$ = 7.3 V ($V_{G1} - V_{G2}$ = 7.4 V). The size of the current window is set to be 0.1 nA ($I_G \pm$ 0.05 nA) which is larger than σ_I at V_G = 0 V. These data are presented in Figure 4c−f. The reflection spectra exhibit their own resonance characteristics for different values of I_G. The resonance frequency and the quality factor of the resonators decrease as I_G increases. This shows that a high I_G leads to an increase in the number of high-energy phonons generated. The averaged reflection spectrum for $V_{G1} - V_{G2}$ = 7.3 V ($V_{G1} - V_{G2}$ = 7.4 V) is the same as the reflection spectrum at I_G = 0.13 nA (I_G = 1.02 nA). This implies that the resonance spectrum fluctuates with the leakage current fluctuations, leading to the noisy spectra shown in Figure 2c and 2d.

The work we present in this study demonstrates the utilization of the gate-controlled supercurrent effect to realize tunable superconducting microwave resonators with enhanced frequency tunability. We achieve a substantial frequency tuning of about 150 MHz (4% shift with respect to the original resonance frequency of our devices), which is comparable to existing methods relying on DC current tuning. Though our tuning method currently exhibits the degradation of internal quality factors, the local voltage tunability has great potential for a wide range of applications based on hybrid quantum devices and superconducting microwave circuits with enhanced device integration. For example, the coupling of microwave and acoustic modes can be switched on/off via local gates in quantum acoustic devices. This will be useful in quantum transduction. Superconducting microwave circuit components like tunable amplifiers, couplers, switches, filters, and impedance-matching circuits could also be promising applications.

To fully utilize this advantage of the GCS-based tuning, further research needs to be carried out. For example, it is strongly desirable to mitigate the quality factor degradation by optimizing the frequency tuning range. An improvement can be made by realizing a microwave resonator with a high internal quality factor ($Q_i > 10^5$) by optimizing fabrication processes so that the internal quality factor remains relatively

https://doi.org/10.1021/acs.nanolett.3c04080
Nano Lett. XXXX, XXX, XXX−XXX

high ($Q_i \sim 10^3$) with a notable frequency shift. This should involve explorations of surface treatment and material deposition conditions. Moreover, the effect of superconducting materials with different critical temperatures on the performance of GCS-based tunable microwave resonators is another important subject for future study. Superconductors with low energy gaps could provide better performance with reduced leakage currents. Changing substrate material, for example, to sapphire also allows us to explore device performance under different GCS mechanisms such as the direct field effect. The utilization of such an effect might lead to tunable resonators with less quality factor degradation by implementing, for example, tunable metallic nanowire Josephson junction whose normal region is controlled via local gating.

AUTHOR INFORMATION

Corresponding Authors

Hyoungsoon Choi − *Department of Physics, Korea Advanced Institute of Science and Technology (KAIST), Daejeon 34141, South Korea; Graduate School of Quantum Science and Technology, Korea Advanced Institute of Science and Technology (KAIST), Daejeon 34141, South Korea*; Email: h.choi@kaist.ac.kr

Jinwoong Cha − *Quantum Technology Institute, Korea Research Institute of Standards and Science (KRISS), Daejeon 34113, South Korea; Graduate School of Quantum Science and Technology, Korea Advanced Institute of Science and Technology (KAIST), Daejeon 34141, South Korea*; orcid.org/0000-0002-1380-4345; Email: chaj@kriss.re.kr

Authors

Younghun Ryu − *Quantum Technology Institute, Korea Research Institute of Standards and Science (KRISS), Daejeon 34113, South Korea; Department of Physics, Korea Advanced Institute of Science and Technology (KAIST), Daejeon 34141, South Korea*

Jinhoon Jeong − *Quantum Technology Institute, Korea Research Institute of Standards and Science (KRISS), Daejeon 34113, South Korea*; orcid.org/0000-0002-8542-5731

Junho Suh − *Department of Physics, Pohang University of Science and Technology (POSTECH), Pohang 37673, South Korea*

Jihwan Kim − *Agency For Defense Development (ADD), Daejeon 34186, South Korea*; orcid.org/0000-0001-9705-423X

Complete contact information is available at: https://pubs.acs.org/10.1021/acs.nanolett.3c04080

Notes

The authors declare no competing financial interest.

ACKNOWLEDGMENTS

We thank the support from the Fab Infra Team at the Quantum Technology Institute of the Korea Research Institute of Standards and Science. J.C. acknowledges support by Korea Research Institute of Standards and Science (Grant KRISS-2023-GP2023-0013), the National Research Council of Science and Technology (NST) (Grant CAP21033-100), and the National Research Foundation of Korea (NRF) (Grant NRF-2022R1C1C1011544) funded by the Korea Government (MSIT). J.S. acknowledges the support from NRF (Grants RS-2023-00207732 and 2022M3H3A1064154) and IITP (Grant IITP-2023-RS-2023-00259676). H.C. acknowledges support by NRF (Grants RS-2023-00207732 and 2022R1A2C2010750) and Korea Basic Science Institute (KBSI) National Research Facilities & Equipment Center (NFEC) grant funded by the Korea Government (MSIT) (Grant PG2022004-09).

REFERENCES

(1) Schoelkopf, R. J.; Girvin, S. M. Wiring up Quantum Systems. *Nature* **2008**, *451* (7179), 664−669.

(2) Zmuidzinas, J. Superconducting Microresonators: Physics and Applications. *Annu. Rev. Condens. Matter Phys.* **2012**, *3* (1), 169−214.

(3) Chuang, I. L.; Computation, Q.; Wineland, D. J.; Blatt, R.; Monroe, C.; Wineland, D. J.; Zoller, P.; Wineland, D. J.; Kirchmair, G.; Roos, C. F.; Blatt, R.; Zoller, P.; Cirac, J. I.; Roos, C. F.; Blatt, R.; Monroe, C.; Zoller, P.; Monroe, C.; Wineland, D. J.; Chuang, I. L.; Irvine, W. T. M.; Cirac, J. I.; Zoller, P.; Maunz, P.; Kim, J.; Cirac, J. I.; Zoller, P.; Jechow, A.; Streed, E. W.; Norton, B. G.; Petrasiunas, M. J.; Kielpinski, D.; Steiner, M.; Meyer, H. M.; Deutsch, C.; Reichel, J.; Monroe, C.; Lattice, O.; Program, E.; Devoret, M. H.; Schoelkopf, R. J. Superconducting Circuits for Quantum Information: An Outlook. *Science* **2013**, *339* (6124), 1169−1174.

(4) Castellanos-Beltran, M. A.; Lehnert, K. W. Widely Tunable Parametric Amplifier Based on a Superconducting Quantum Interference Device Array Resonator. *Appl. Phys. Lett.* **2007**, *91* (8), 083509.

(5) Yamamoto, T.; Inomata, K.; Watanabe, M.; Matsuba, K.; Miyazaki, T.; Oliver, W. D.; Nakamura, Y.; Tsai, J. S. Flux-Driven Josephson Parametric Amplifier. *Appl. Phys. Lett.* **2008**, *93* (4), 042510.

(6) Castellanos-Beltran, M. A.; Irwin, K. D.; Hilton, G. C.; Vale, L. R.; Lehnert, K. W. Amplification and Squeezing of Quantum Noise with a Tunable Josephson Metamaterial. *Nat. Phys.* **2008**, *4* (12), 929−931.

(7) McKay, D. C.; Filipp, S.; Mezzacapo, A.; Magesan, E.; Chow, J. M.; Gambetta, J. M. Universal Gate for Fixed-Frequency Qubits via a Tunable Bus. *Phys. Rev. Appl.* **2016**, *6* (6), 064007.

(8) Schuster, D. I.; Sears, A. P.; Ginossar, E.; Dicarlo, L.; Frunzio, L.; Morton, J. J. L.; Wu, H.; Briggs, G. A. D.; Buckley, B. B.; Awschalom, D. D.; Schoelkopf, R. J. High-Cooperativity Coupling of Electron-Spin Ensembles to Superconducting Cavities. *Phys. Rev. Lett.* **2010**, *105* (14), 140501.

(9) Mi, X.; Benito, M.; Putz, S.; Zajac, D. M.; Taylor, J. M.; Burkard, G.; Petta, J. R. A Coherent Spin-Photon Interface in Silicon. *Nature* **2018**, *555* (7698), 599−603.

(10) Samkharadze, N.; Zheng, G.; Kalhor, N.; Brousse, D.; Sammak, A.; Mendes, U. C.; Blais, A.; Scappucci, G.; Vandersypen, L. M. K. Strong Spin-Photon Coupling in Silicon. *Science (80-.).* **2018**, *359* (6380), 1123−1127.

(11) Bolgar, A. N.; Zotova, J. I.; Kirichenko, D. D.; Besedin, I. S.; Semenov, A. V.; Shaikhaidarov, R. S.; Astafiev, O. V. Quantum Regime of a Two-Dimensional Phonon Cavity. *Phys. Rev. Lett.* **2018**, *120* (22), 223603.

(12) Moores, B. A.; Sletten, L. R.; Viennot, J. J.; Lehnert, K. W. Cavity Quantum Acoustic Device in the Multimode Strong Coupling Regime. *Phys. Rev. Lett.* **2018**, *120* (22), 227701.

(13) Satzinger, K. J.; Zhong, Y. P.; Chang, H. S.; Peairs, G. A.; Bienfait, A.; Chou, M. H.; Cleland, A. Y.; Conner, C. R.; Dumur; Grebel, J.; Gutierrez, I.; November, B. H.; Povey, R. G.; Whiteley, S. J.; Awschalom, D. D.; Schuster, D. I.; Cleland, A. N. Quantum Control of Surface Acoustic-Wave Phonons. *Nature* **2018**, *563* (7733), 661−665.

(14) Huebl, H.; Zollitsch, C. W.; Lotze, J.; Hocke, F.; Greifenstein, M.; Marx, A.; Gross, R.; Goennenwein, S. T. B. High Cooperativity in Coupled Microwave Resonator Ferrimagnetic Insulator Hybrids. *Phys. Rev. Lett.* **2013**, *111* (12), 127003.

(15) Zhang, X.; Zou, C. L.; Jiang, L.; Tang, H. X. Strongly Coupled Magnons and Cavity Microwave Photons. *Phys. Rev. Lett.* **2014**, *113* (15), 156401.
(16) Tabuchi, Y.; Ishino, S.; Ishikawa, T.; Yamazaki, R.; Usami, K.; Nakamura, Y. Hybridizing Ferromagnetic Magnons and Microwave Photons in the Quantum Limit. *Phys. Rev. Lett.* **2014**, *113* (8), 083603.
(17) Dolan, G. J.; You, A.; Be, M.; In, I. Offset Masks for Lift off Photoprocessing. *Appl. Phys. Lett.* **1977**, *31* (5), 337−339.
(18) Osman, A.; Simon, J.; Bengtsson, A.; Kosen, S.; Krantz, P.; P. Lozano, D.; Scigliuzzo, M.; Delsing, P.; Bylander, J.; Fadavi Roudsari, A. Simplified Josephson-Junction Fabrication Process for Reproducibly High-Performance Superconducting Qubits. *Appl. Phys. Lett.* **2021**, *118* (6), 064002.
(19) Larsen, T. W.; Petersson, K. D.; Kuemmeth, F.; Jespersen, T. S.; Krogstrup, P.; Nygård, J.; Marcus, C. M. Semiconductor-Nanowire-Based Superconducting Qubit. *Phys. Rev. Lett.* **2015**, *115* (12), 127001.
(20) Casparis, L.; Larsen, T. W.; Olsen, M. S.; Kuemmeth, F.; Krogstrup, P.; Nygård, J.; Petersson, K. D.; Marcus, C. M. Gatemon Benchmarking and Two-Qubit Operations. *Phys. Rev. Lett.* **2016**, *116* (15), 150505.
(21) Casparis, L.; Connolly, M. R.; Kjaergaard, M.; Pearson, N. J.; Kringhøj, A.; Larsen, T. W.; Kuemmeth, F.; Wang, T.; Thomas, C.; Gronin, S.; Gardner, G. C.; Manfra, M. J.; Marcus, C. M.; Petersson, K. D. Superconducting Gatemon Qubit Based on a Proximitized Two-Dimensional Electron Gas. *Nat. Nanotechnol.* **2018**, *13* (10), 915−919.
(22) Sarkar, J.; Salunkhe, K. V.; Mandal, S.; Ghatak, S.; Marchawala, A. H.; Das, I.; Watanabe, K.; Taniguchi, T.; Vijay, R.; Deshmukh, M. M. Quantum-Noise-Limited Microwave Amplification Using a Graphene Josephson Junction. *Nat. Nanotechnol.* **2022**, *17* (11), 1147−1152.
(23) Butseraen, G.; Ranadive, A.; Aparicio, N.; Rafsanjani Amin, K.; Juyal, A.; Esposito, M.; Watanabe, K.; Taniguchi, T.; Roch, N.; Lefloch, F.; Renard, J. A Gate-Tunable Graphene Josephson Parametric Amplifier. *Nat. Nanotechnol.* **2022**, *17* (11), 1153−1158.
(24) Antipov, A. E.; Bargerbos, A.; Winkler, G. W.; Bauer, B.; Rossi, E.; Lutchyn, R. M. Effects of Gate-Induced Electric Fields on Semiconductor Majorana Nanowires. *Phys. Rev. X* **2018**, *8* (3), 031041.
(25) Mikkelsen, A. E. G.; Kotetes, P.; Krogstrup, P.; Flensberg, K. Hybridization at Superconductor-Semiconductor Interfaces. *Phys. Rev. X* **2018**, *8* (3), 031040.
(26) De Moor, M. W. A.; Bommer, J. D. S.; Xu, D.; Winkler, G. W.; Antipov, A. E.; Bargerbos, A.; Wang, G.; Loo, N. v.; Op Het Veld, R. L. M.; Gazibegovic, S.; Car, D.; Logan, J. A.; Pendharkar, M.; Lee, J. S.; M Bakkers, E. P. A.; Palmstrom, C. J.; Lutchyn, R. M.; Kouwenhoven, L. P.; Zhang, H. Electric Field Tunable Superconductor-Semiconductor Coupling in Majorana Nanowires. *New J. Phys.* **2018**, *20* (10), 103049.
(27) Splitthoff, L. J.; Bargerbos, A.; Grünhaupt, L.; Pita-Vidal, M.; Wesdorp, J. J.; Liu, Y.; Kou, A.; Andersen, C. K.; Van Heck, B. Gate-Tunable Kinetic Inductance in Proximitized Nanowires. *Phys. Rev. Appl.* **2022**, *18* (2), 024074.
(28) Splitthoff, L. J.; Wesdorp, J. J.; Pita-Vidal, M.; Bargerbos, A.; Andersen, C. K. Gate-Tunable Kinetic Inductance Parametric Amplifier. *arXiv* **2023**, 2308.06989.
(29) De Simoni, G.; Paolucci, F.; Solinas, P.; Strambini, E.; Giazotto, F. Metallic Supercurrent Field-Effect Transistor. *Nat. Nanotechnol.* **2018**, *13* (9), 802−805.
(30) Paolucci, F.; Vischi, F.; De Simoni, G.; Guarcello, C.; Solinas, P.; Giazotto, F. Field-Effect Controllable Metallic Josephson Interferometer. *Nano Lett.* **2019**, *19* (9), 6263−6269.
(31) Paolucci, F.; Crisá, F.; De Simoni, G.; Bours, L.; Puglia, C.; Strambini, E.; Roddaro, S.; Giazotto, F. Electrostatic Field-Driven Supercurrent Suppression in Ionic-Gated Metallic Superconducting Nanotransistors. *Nano Lett.* **2021**, *21* (24), 10309−10314.
(32) Basset, J.; Stanisavljević, O.; Kuzmanović, M.; Gabelli, J.; Quay, C. H. L.; Estève, J.; Aprili, M. Gate-Assisted Phase Fluctuations in All-Metallic Josephson Junctions. *Phys. Rev. Res.* **2021**, *3* (4), 043169.
(33) Ritter, M. F.; Crescini, N.; Haxell, D. Z.; Hinderling, M.; Riel, H.; Bruder, C.; Fuhrer, A.; Nichele, F. Out-of-Equilibrium Phonons in Gated Superconducting Switches. *Nat. Electron.* **2022**, *5* (2), 71−77.
(34) Catto, G.; Liu, W.; Kundu, S.; Lahtinen, V.; Vesterinen, V.; Möttönen, M. Microwave Response of a Metallic Superconductor Subject to a High-Voltage Gate Electrode. *Sci. Rep.* **2022**, *12* (1), 6822.
(35) Bours, L.; Mercaldo, M. T.; Cuoco, M.; Strambini, E.; Giazotto, F. Unveiling Mechanisms of Electric Field Effects on Superconductors by a Magnetic Field Response. *Phys. Rev. Res.* **2020**, *2* (3), 033353.
(36) Puglia, C.; De Simoni, G.; Ligato, N.; Giazotto, F. Vanadium Gate-Controlled Josephson Half-Wave Nanorectifier. *Appl. Phys. Lett.* **2020**, *116* (25), 252601.
(37) Puglia, C.; De Simoni, G.; Giazotto, F. Electrostatic Control of Phase Slips in Ti Josephson Nanotransistors. *Phys. Rev. Appl.* **2020**, *13* (5), 054026.
(38) Rocci, M.; De Simoni, G.; Giazotto, F.; Puglia, C.; Esposti, D. D.; Strambini, E.; Zannier, V.; Sorba, L. Gate-Controlled Suspended Titanium Nanobridge Supercurrent Transistor. *ACS Nano* **2020**, *14* (10), 12621−12628.
(39) De Simoni, G.; Puglia, C.; Giazotto, F. Niobium Dayem Nano-Bridge Josephson Gate-Controlled Transistors. *Appl. Phys. Lett.* **2020**, *116* (24), 242601.
(40) Ritter, M. F.; Fuhrer, A.; Haxell, D. Z.; Hart, S.; Gumann, P.; Riel, H.; Nichele, F. A Superconducting Switch Actuated by Injection of High-Energy Electrons. *Nat. Commun.* **2021**, *12* (1), 1266.
(41) Golokolenov, I.; Guthrie, A.; Kafanov, S.; Pashkin, Y. A.; Tsepelin, V. On the Origin of the Controversial Electrostatic Field Effect in Superconductors. *Nat. Commun.* **2021**, *12* (1), 2747.
(42) Elalaily, T.; Kürtössy, O.; Scherübl, Z.; Berke, M.; Fülöp, G.; Lukács, I. E.; Kanne, T.; Nygård, J.; Watanabe, K.; Taniguchi, T.; Makk, P.; Csonka, S. Gate-Controlled Supercurrent in Epitaxial Al/InAs Nanowires. *Nano Lett.* **2021**, *21* (22), 9684−9690.
(43) Alegria, L. D.; Bøttcher, C. G. L.; Saydjari, A. K.; Pierce, A. T.; Lee, S. H.; Harvey, S. P.; Vool, U.; Yacoby, A. High-Energy Quasiparticle Injection into Mesoscopic Superconductors. *Nat. Nanotechnol.* **2021**, *16* (4), 404−408.
(44) Sandberg, M.; Vissers, M. R.; Kline, J. S.; Weides, M.; Gao, J.; Wisbey, D. S.; Pappas, D. P. Etch Induced Microwave Losses in Titanium Nitride Superconducting Resonators. *Appl. Phys. Lett.* **2012**, *100* (26), 262605.
(45) Probst, S.; Song, F. B.; Bushev, P. A.; Ustinov, A. V.; Weides, M. Efficient and Robust Analysis of Complex Scattering Data under Noise in Microwave Resonators. *Rev. Sci. Instrum.* **2015**, *86* (2), 024706.
(46) Mattis, D. C.; Bardeen, J. Theory of the Anomalous Skin Effect in Normal and Superconducting Metals. *Phys. Rev.* **1958**, *111* (2), 412−417.
(47) De Tomas, C.; Cantarero, A.; Lopeandia, A. F.; Alvarez, F. X. From Kinetic to Collective Behavior in Thermal Transport on Semiconductors and Semiconductor Nanostructures. *J. Appl. Phys.* **2014**, *115* (16), 164314.
(48) Gao, J. The Physics of Superconducting Microwave Resonators. Ph.D. Thesis, California Institute of Technology, 2008.
(49) Vissers, M. R.; Hubmayr, J.; Sandberg, M.; Chaudhuri, S.; Bockstiegel, C.; Gao, J. Frequency-Tunable Superconducting Resonators via Nonlinear Kinetic Inductance. *Appl. Phys. Lett.* **2015**, *107* (6), 62601.
(50) Xu, M.; Han, X.; Fu, W.; Zou, C. L.; Devoret, M. H.; Tang, H. X. Frequency-Tunable High- Q Superconducting Resonators via Wireless Control of Nonlinear Kinetic Inductance. *Appl. Phys. Lett.* **2019**, *114* (19), 192601.
(51) Owen, C. S.; Scalapino, D. J. Superconducting State under the Influence of External Dynamic Pair Breaking. *Phys. Rev. Lett.* **1972**, *28* (24), 1559−1561.

https://doi.org/10.1021/acs.nanolett.3c04080
Nano Lett. XXXX, XXX, XXX−XXX

(52) Gao, J.; Zmuidzinas, J.; Vayonakis, A.; Day, P.; Mazin, B.; Leduc, H. Equivalence of the Effects on the Complex Conductivity of Superconductor Due to Temperature Change and External Pair Breaking. *J. Low Temp. Phys.* **2008**, *151* (1−2), 557−563.
(53) Gao, J.; Vissers, M. R.; Sandberg, M. O.; Da Silva, F. C. S.; Nam, S. W.; Pappas, D. P.; Wisbey, D. S.; Langman, E. C.; Meeker, S. R.; Mazin, B. A.; Leduc, H. G.; Zmuidzinas, J.; Irwin, K. D. A Titanium-Nitride near-Infrared Kinetic Inductance Photon-Counting Detector and Its Anomalous Electrodynamics. *Appl. Phys. Lett.* **2012**, *101* (14), 142602.
(54) Chawla, J. S.; Zhang, X. Y.; Gall, D. Effective Electron Mean Free Path in TiN(001). *J. Appl. Phys.* **2013**, *113* (6), 063704.
(55) Pracht, U. S.; Scheffler, M.; Dressel, M.; Kalok, D. F.; Strunk, C.; Baturina, T. I. Direct Observation of the Superconducting Gap in a Thin Film of Titanium Nitride Using Terahertz Spectroscopy. *Phys. Rev. B - Condens. Matter Mater. Phys.* **2012**, *86* (18), 184503.
(56) Tinkham, M. *Introduction to Superconductivity*; Courier Corporation, 2004.
(57) Mazin, B. A. Microwave Kinetic Inductance Detectors, Ph.D. Thesis, California Institute of Technology, 2005.
(58) Anufriev, R.; Ordonez-Miranda, J.; Nomura, M. Measurement of the Phonon Mean Free Path Spectrum in Silicon Membranes at Different Temperatures Using Arrays of Nanoslits. *Phys. Rev. B* **2020**, *101* (11), 115301.
(59) Minnich, A. J.; Johnson, J. A.; Schmidt, A. J.; Esfarjani, K.; Dresselhaus, M. S.; Nelson, K. A.; Chen, G. Thermal Conductivity Spectroscopy Technique to Measure Phonon Mean Fee Paths. *Phys. Rev. Lett.* **2011**, *107* (9), 095901.

https://doi.org/10.1021/acs.nanolett.3c04080
Nano Lett. XXXX, XXX, XXX−XXX